International Journal of Bifurcation and Chaos, Vol. 15, No. 1 (2005) 65–82

PERFORMANCE OF AN AUTOMATIC BALL BALANCER WITH DRY FRICTION

N. VAN DE WOUW*, M. N. VAN DEN HEUVEL and H. NIJMEIJER
Department of Mechanical Engineering, Eindhoven University of Technology, P.O. Box 513, 5600 MB Eindhoven, The Netherlands
**N.v.d.Wouw@tue.nl*

J. A. VAN ROOIJ
Philips Components, Philips Optical Storage, P.O. Box 80002, 5600 JB Eindhoven, The Netherlands

Received February 26, 2004; Revised April 15, 2004

In many industrial applications imbalance is a major cause for unwanted vibrations. One way to compensate for an unknown imbalance is the implementation of an automatic ball balancer. Oil-lubricated automatic ball balancers are applied in hand-held tools and washers. However, in applications such as optical drives fluid lubrication is highly undesirable since it may destroy the optical system upon leakage. Therefore, in this paper, the balancing performance of an automatic ball balancer without fluid lubrication is investigated. The absence of fluid lubrication gives rise to dry friction phenomena which cause the existence of equilibrium sets of the balls in the automatic ball balancer. A model of the system with dry friction, modeled by a set-valued force law, is built based on dedicated experiments. The resulting equilibrium sets and their dependency on system parameters are studied and the consequences for the balancing performance is assessed. Based on these results, it can be concluded that in parts of such equilibrium sets the balancing performance deteriorates when compared to the system without automatic ball balancer; in other words, the balancing performance is endangered by the presence of dry friction. This conclusion is supported by both numerical and experimental results.

Keywords: Optical storage drives; discontinuous dynamics; equilibrium sets; Coulomb friction.

1. Introduction

In machines with rotating components, imbalance is one of the main engineering problems since it causes unwanted vibrations. One solution to this problem is the application of an automatic ball balancer (ABB). In principle, an ABB is capable of counteracting the imbalance, even when the imbalance is *a priori* unknown. An example of an industrial application in which an ABB is implemented is a DVD-drive, see Fig. 1. In this figure, part of a DVD-drive is shown, with the optical lens and the ABB. In such a system, unwanted vibrations due to imbalances will seriously deteriorate the tracking performance of the optical system. The imbalance is present on the DVD disc due to production imperfections. Both the size and location of this imbalance are unknown and can vary per disc. The ABB consists of a rim with a number of balls, which will — in a certain range of rotating frequencies of the motor — be positioned such that the imbalance is counteracted. In this way, the ABB can, to a certain extent, adapt automatically to counteract the unknown imbalance. The study of the dynamic behavior of automatic ball balancers was initialized by Thearle [1950]. Other systems in which automatic ball balancers are used are washing machines and hand-held tools [Rajalingham & Rakheja, 1998; Lindell, 1996]. In the latter applications, often a

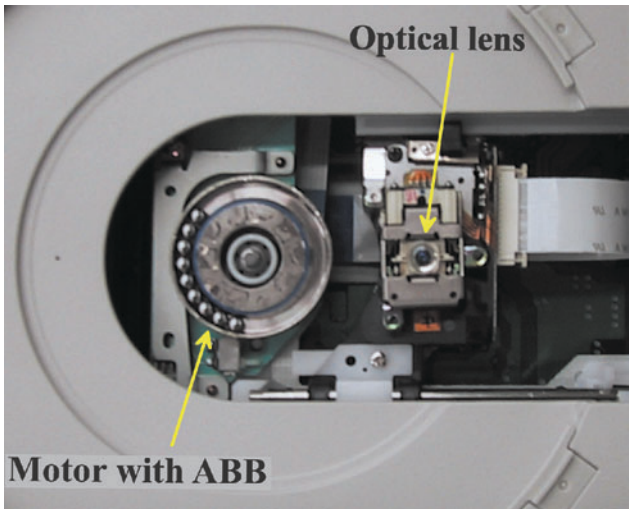

Fig. 1. Example of an Automatic Ball Balancer, mounted on a DVD-ROM drive.

viscous fluid is present in the ABB, ensuring that only viscous friction forces between the balls and the rim are present. The resulting dissipative forces acting on the balls are necessary to ensure the stability of the balancing positions of the balls. These balancing positions of the balls are equilibria in which the balls stand still with respect to the rim of the ABB. In literature, the vast majority of the research on ABBs has focussed on fluid-lubricated ABBs, see for example [Lee, 1995; Lee & Moorhem, 1996; Chung & Ro, 1999; Chung & Jang, 2003; Gorbenko, 2003]. However, in a DVD-drive the use of fluids is highly undesirable, since leakage would destroy the optical system. Without fluid, the dry friction between rim and balls induces the dissipative forces necessary to stabilize the balancing positions of the balls. In [Huang *et al.*, 2002a, 2002b], an ABB for optic disc drives without damping fluid and one ball is studied. Herein, the negative effect of a rolling friction force on the balancing performance was indicated. As will be shown in this paper, the balancing performance of the ABB can be seriously affected by the stiction behavior related to the dry friction present between the rim and the balls, because this stiction phenomenon leads to the existence of equilibrium *sets*. In other words, the balls can come to a standstill in a range of positions, some of which do not necessarily lead to balancing.

So, the main research question of this paper is the assessment of the performance of an automatic ball balancer with dry friction. More specifically, we aim to assess the influence of the dry friction on the balancing performance.

In Sec. 2, the experimental setup is introduced. A model of this setup will be presented in Sec. 3, where a set-valued force law is used to model the friction in order to account for the stiction phenomenon mentioned above. Section 4 is devoted to the working principle of the ABB and explains how this is endangered by the presence of dry friction. In Sec. 5, the equilibrium sets of the model are determined and their dependency on system parameters, such as the friction coefficient and the rotational speed of the ABB, is investigated. The consequences regarding the balancing performance of the ABB are discussed and a confrontation with experimental results is presented. In Sec. 6, the static friction parameter of the friction model is identified by means of dedicated experiments for a specific choice of the material types of the rim of the ABB and the balls. Moreover, the consequences in terms of the equilibrium sets and the resulting balancing performance of the ABB for this specific friction situation are investigated. Finally, conclusions are presented in Sec. 7.

2. The Experimental Setup

The experimental setup incorporating an ABB in a CDROM system is depicted in Fig. 2. In this experimental system only two balls are present, see also Fig. 3. The ABB is mounted on a table that is suspended by four wits. These supporting wits represent the suspension of the motor and ABB in a real CDROM player. Moreover, at the bottom of the table a rod is attached, which is submerged into a vessel with oil. The extent to which the rod is submerged and the type of fluid will determine the viscous damping forces invoked at the suspension of the table. The motor that drives the ABB is attached to the table. The ABB is rigidly attached to the rotor part of the motor via the motor shaft, which drives the CD with a known angular velocity. Moreover, a CD disc is attached rigidly to the motor. At discrete locations on the disc, small screws can be mounted to the disc. In this way, imbalances of different magnitude and location can be added in a well-defined and reproducible way. The ABB contains only two balls, since this significantly simplifies the modeling and analysis of this system, but still allows for the illustration of the effect of dry friction on the performance of the

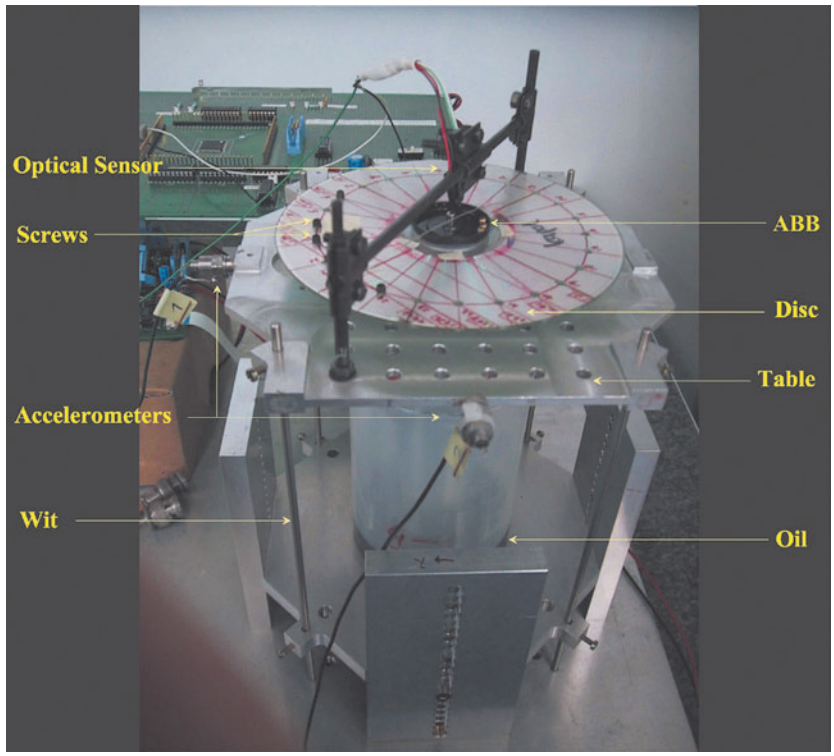

Fig. 2. Picture of the experimental setup.

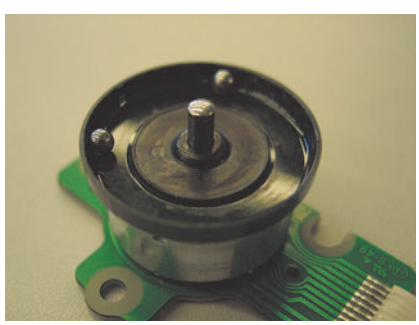

Fig. 3. ABB with two balls.

system. For an analysis of the dynamic behavior of an oil-filled automatic balancer with more than two balls see [Lee & Moorhem, 1996].

The measurement equipment used in this setup consists of two accelerometers used to measure the accelerations of the table in the horizontal plane and a rotational encoder in the motor, which measures the angular displacement of the motor (disc and ABB). Moreover, the angular positions of the two balls (and the imbalance) are measured using an optical sensor and a high-speed camera, see Sec. 6.

3. Model of the ABB

A schematic representation of the experimental setup is depicted in Fig. 4. Herein, it is assumed that all movements are in the horizontal plane and that the table does not rotate (see [Bövik & Högfors, 1986] for a study on an ABB in a nonplanar rotor). The four wits supporting the table and the rod submerged in oil can be modeled by two linear springs and dampers, positioned perpendicular to each other (stiffness parameters k_1 and k_2 and damping parameters b_1 and b_2), attached on one end to the table and on the other end to inertial space. In this paper, we will only consider the case of an isotropic suspension of the table: $k := k_1 = k_2$ and $b := b_1 = b_2$. See [Wettergren, 2001] for a study of the dynamic behavior of an ABB with an anisotropic suspension. In Fig. 4, point A is a fixed point in space, which coincides with point B when the system is at rest. Recall that the motor drives the ABB and the disc with a known angular velocity $\Omega(t)$. From now on we will consider only constant driving velocities Ω, since we are mainly interested in the steady-state behavior (the equilibrium set) of the system. The total mass of the table, motor and ABB (without the balls) and the CD

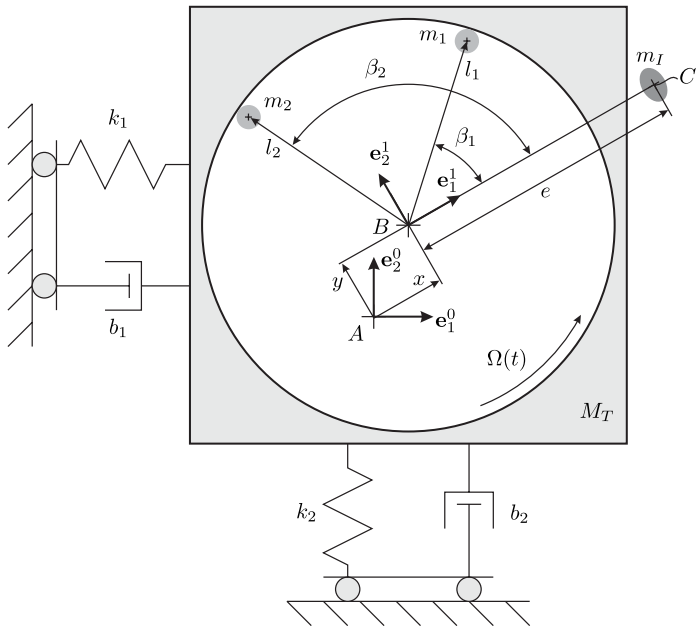

Fig. 4. Schematic representation of the experimental setup with the Automatic Ball Balancer.

(without the imbalance) is called M_T. The imbalance is modeled as a point-mass in point C with mass m_I. The distance between the geometrical center of the ABB (point B) to the imbalance (point C) is called e. The ABB contains two identical balls, each having mass m_i, $i = 1, 2$. These balls are free to move along the rim of the ABB. It is assumed that, under the influence of centrifugal forces, the balls are always in contact with the rim. The distance between the geometrical center of the ABB to the center of ball i is called l_i. Between the balls and the rim, friction (rolling friction) is present, resulting in friction forces in tangential direction. It should be noted that in the current model contact between the balls is not modeled.

A model of the experimental system is derived and can be formulated in terms of the generalized coordinates $\underline{q} = [x \quad y \quad \beta_1 \quad \beta_2 \quad l_1 \quad l_2]^T$, see Fig. 4. Herein, x and y are defined by $\mathbf{r}_{B/A} = [x \quad y]\underline{\mathbf{e}}^1$, where $\mathbf{r}_{B/A}$ is the position vector of point B with respect to point A and $\underline{\mathbf{e}}^1 = [\mathbf{e}_1^1 \quad \mathbf{e}_2^1]^T$. Moreover, the rotating body-fixed frame $\underline{\mathbf{e}}^1$ is related to the inertial frame $\underline{\mathbf{e}}^0$ by:

$$\underline{\mathbf{e}}^1 = \begin{bmatrix} \cos(\theta(t)) & \sin(\theta(t)) \\ -\sin(\theta(t)) & \cos(\theta(t)) \end{bmatrix} \underline{\mathbf{e}}^0, \tag{1}$$

in which $\theta(t) = \Omega\, t + \theta(0)$ expresses the angular displacement of the motor. The coordinates l_i, $i = 1, 2$, define the distance between the center of ball i and point B and β_i, $i = 1, 2$, define the angular position of ball i relative to the imbalance at point C. Using a Lagrangian approach, the equations of motion are derived:

$$\underline{M}(\underline{q})\ddot{\underline{q}} - \underline{h}\left(\underline{q}, \dot{\underline{q}}\right) = \underline{W}_T\underline{\lambda}_T + \underline{W}_N\underline{\lambda}_N, \tag{2}$$

$$\underline{g}_N(\underline{q}) = \underline{0}, \tag{3}$$

where

$$\underline{M}(\underline{q}) = \begin{bmatrix} M & 0 & -m_1 l_1 \sin\beta_1 & -m_2 l_2 \sin\beta_2 & m_1\cos\beta_1 & m_2\cos\beta_2 \\ 0 & M & m_1 l_1 \cos\beta_1 & m_2 l_2 \cos\beta_2 & m_1\sin\beta_1 & m_2\sin\beta_2 \\ -m_1 l_1 \sin\beta_1 & m_1 l_1\cos\beta_1 & m_1 l_1^2 + J_1\left(\dfrac{2l_1}{d_1}\right)^2 & 0 & 0 & 0 \\ -m_2 l_2 \sin\beta_2 & m_2 l_2\cos\beta_2 & 0 & m_2 l_2^2 + J_2\left(\dfrac{2l_2}{d_2}\right)^2 & 0 & 0 \\ m_1\cos\beta_1 & m_1\sin\beta_1 & 0 & 0 & m_1 & 0 \\ m_2\cos\beta_2 & m_2\sin\beta_2 & 0 & 0 & 0 & m_2 \end{bmatrix},$$

$$\underline{W}_T = \begin{bmatrix} 0 & 0 \\ 0 & 0 \\ 1 & 0 \\ 0 & 1 \\ 0 & 0 \\ 0 & 0 \end{bmatrix}, \quad \underline{W}_N = \begin{bmatrix} 0 & 0 \\ 0 & 0 \\ 0 & 0 \\ 0 & 0 \\ -1 & 0 \\ 0 & -1 \end{bmatrix}, \quad \underline{g}_N(\underline{q}) = \begin{bmatrix} -l_1 + L \\ -l_2 + L \end{bmatrix},$$

$\underline{h}(\underline{q}, \underline{\dot{q}}) = [h_x \;\; h_y \;\; h_{\beta_1} \;\; h_{\beta_2} \;\; h_{l_1} \;\; h_{l_2}]^T$, with:

$$\begin{aligned}
h_x &= -\Big\{ -2M\omega\dot{y} - M\omega^2 x - m_I e\omega^2 \\
&\quad -\Big(m_1 l_1 \cos\beta_1 (\dot{\beta}_1 + \omega)^2 + m_2 l_2 \cos\beta_2 (\dot{\beta}_2 + \omega)^2\Big) + kx + b(\dot{x} - \omega y)\Big\}, \\
h_y &= -\Big\{ 2M\omega\dot{x} - M\omega^2 y \\
&\quad -\Big(m_1 l_1 \sin\beta_1 (\dot{\beta}_1 + \omega)^2 + m_2 l_2 \sin\beta_2 (\dot{\beta}_2 + \omega)^2\Big) + ky + b(\dot{y} + \omega x)\Big\}, \\
h_{\beta_1} &= -\Big\{ 2m_1 l_1 \omega\dot{x}\cos\beta_1 + 2m_1 l_1 \omega\dot{y}\sin\beta_1 + m_1 l_1 \omega^2 x \sin\beta_1 - m_1 l_1 \omega^2 y \cos\beta_1 \Big\}, \\
h_{\beta_2} &= -\Big\{ 2m_2 l_2 \omega\dot{x}\cos\beta_2 + 2m_2 l_2 \omega\dot{y}\sin\beta_2 + m_2 l_2 \omega^2 x \sin\beta_2 - m_2 l_2 \omega^2 y \cos\beta_2 \Big\}, \\
h_{l_1} &= -\Big\{ 2m_1 \omega \sin\beta_1 \dot{x} - 2m_1 \omega \cos\beta_1 \dot{y} - m_1 \omega^2 \cos\beta_1 x - m_1 \omega^2 \sin\beta_1 y \\
&\quad - m_1 l_1 (\dot{\beta}_1 + \omega)^2 - \frac{2J_1}{d_1}\left(\frac{2l_1}{d_1}\dot{\beta}_1 - \omega\right)\dot{\beta}_1 \Big\}, \\
h_{l_2} &= -\Big\{ 2m_2 \omega \sin\beta_2 \dot{x} - 2m_2 \omega \cos\beta_2 \dot{y} - m_2 \omega^2 \cos\beta_2 x - m_2 \omega^2 \sin\beta_2 y \\
&\quad - m_2 l_2 (\dot{\beta}_2 + \omega)^2 - \frac{2J_2}{d_2}\left(\frac{2l_2}{d_2}\dot{\beta}_2 - \omega\right)\dot{\beta}_2 \Big\}.
\end{aligned}$$

Herein, $M = M_T + m_I + m_1 + m_2$, d_i is the diameter of ball i and J_i is the moment of inertia of ball i about an axis perpendicular to the plane of the ABB and through the center of mass of ball i. Moreover, $\underline{\lambda}_N = [F_{N_1} \;\; F_{N_2}]^T$ is a column of Lagrange multipliers related to the normal forces between the balls and the rim of the automatic ball balancer (F_{N_i} is the normal force between ball i and the rim) and $\underline{\lambda}_T = [F_{T_1} \;\; F_{T_2}]^T$ is a column of Lagrange multipliers related to the friction forces between the balls and the rim of the auto-balancing unit (F_{T_i} is the friction force between ball i and the rim). It should be noted that the constraint forces in $\underline{\lambda}_N$ ensure the satisfaction of the holonomic, bilateral constraints expressed by (3): $l_i = L$, $i = 1, 2$, where L is a constant. These constraints express that the balls stay in touch with the rim at all times.

Moreover, the friction forces are modeled using a set-valued force law in order to account for the stiction behavior which is observed in the experiments:

$$F_{T_i} \in -\mu_i |F_{N_i}| \,\mathrm{Sign}(\dot{\beta}_i), \quad i = 1, 2. \tag{4}$$

Herein, $\mathrm{Sign}(x)$ is the set-valued sign-function

$$\mathrm{Sign}(x) = \begin{cases} \{-1\} & x < 0 \\ [-1, 1] & x = 0 \\ \{1\} & x > 0 \end{cases} \tag{5}$$

and μ_i is the friction coefficient related to the contact between ball i and the rim. It should

Table 1. Estimated parameter values.

Parameter	Value		Parameter	Value	
M_T	$3.24 \cdot 10^{-1}$	[kg]	b	1.28	[N s/m]
k	$1.07 \cdot 10^{4}$	[N/m]	L	$1.15 \cdot 10^{-2}$	[m]
m_1	$1.4 \cdot 10^{-4}$	[kg]	m_2	$1.4 \cdot 10^{-4}$	[kg]
d_1	$3.0 \cdot 10^{-3}$	[m]	d_2	$3.0 \cdot 10^{-3}$	[m]
m_I	$5.6 \cdot 10^{-4}$	[kg]	e	$3.7 \cdot 10^{-3}$	[m]

be noted that now the model, described by (2) and (4) is formulated as a differential inclusion. Note that (4) expresses a Coulomb friction model. At this point, more complex friction modeling for nonzero velocities is not pursued since the main focus of this paper is on the analysis of the equilibrium sets of the system. Namely, one should realize that these equilibrium sets are only (as far as the friction model is concerned) determined by the static friction level and not by the friction model for nonzero velocities.

Dedicated experiments were performed to estimate all the parameters in the model, except the friction coefficients; the estimation of the friction coefficients will be discussed in Sec. 6. Table 1 shows the estimated parameter values.

The masses m_i of balls and m_I of the imbalances, the diameters of the balls d_i and the unbalance location (characterized by e) are measured directly. Moreover, the parameters M_T, k and b are estimated based on a measured frequency response function between a force acting on the table (including CD, imbalance and ABB) and the acceleration of the table. It should be noted that in spite of the fact that it is possible to change the imbalance present on the disc by replacing the screws in the CD, the values of m_I and e are kept constant throughout the work presented in this paper.

4. Working Principle of the ABB

Before the dynamics of the system with dry friction is investigated in the next sections, in this section the working principle of the ABB is illuminated. The working principle of an ABB can be explained using Fig. 5. Herein, the total imbalance, which is the resultant of the imbalances due to m_I in C and the balls, is located in point Γ. Note that, when the movements of the balls are neglected, this model is identical to the Jeffcott rotor model [Childs, 1993]. It is known from the Jeffcott model that, when the

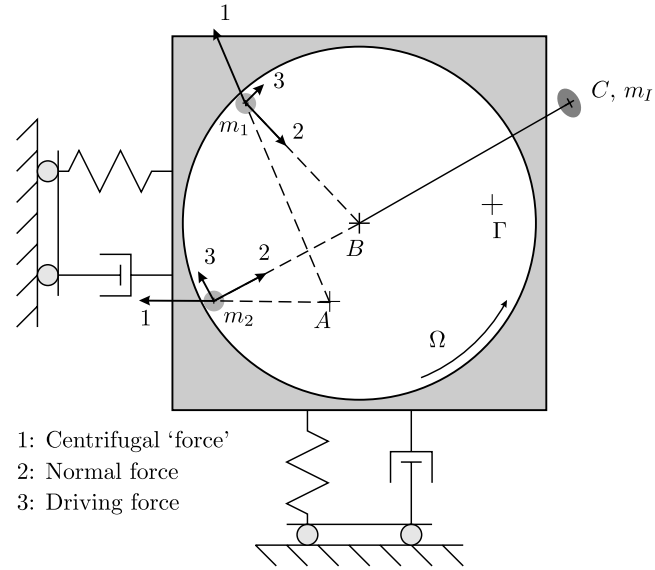

Fig. 5. Working principle of the ABB.

rotor has a constant speed Ω, it experiences a synchronous — at the same rotational velocity as the rotational velocity Ω — motion called whirl in a circular orbit due to the imbalance in Γ. The ABB exhibits the same type of behavior: in Fig. 5, the center of the circular orbit is point A, which is fixed to inertial space. Points A and B coincide when the ABB is at rest ($\Omega = 0$) or when the system is completely balanced.

The behavior of the balls can now be explained by investigation of the interplay of forces acting on the balls. Firstly, the centrifugal "force" is directed along the line from A to m_i. The word "force" is put between quotation marks, because it is of course only an *apparent* force, experienced by a mass when it moves along a curved line, due to inertia effects. Secondly, a normal force (constraint force due to constraints (3)) acts on the ball, exerted by the rim of the ABB. The normal force is directed locally perpendicular to the contact surface, so towards point B. The resultant of these two forces is a tangential force, which excites the balls. Therefore, this resultant force will be called the *driving force*.

Now, let us explain when the balls are driven to such positions that result in balancing of the system. The Jeffcott model provides the clue. Namely, when the rotational speed of the system is below the so-called critical speed of the system, the rotor is in phase with the imbalance vector $\mathbf{r}_{\Gamma/B}$, pointing from B to Γ, while above the critical speed, the rotor is 180° out of phase with $\mathbf{r}_{\Gamma/B}$, see Figs. 6 and 7, respectively. Therefore, below the critical

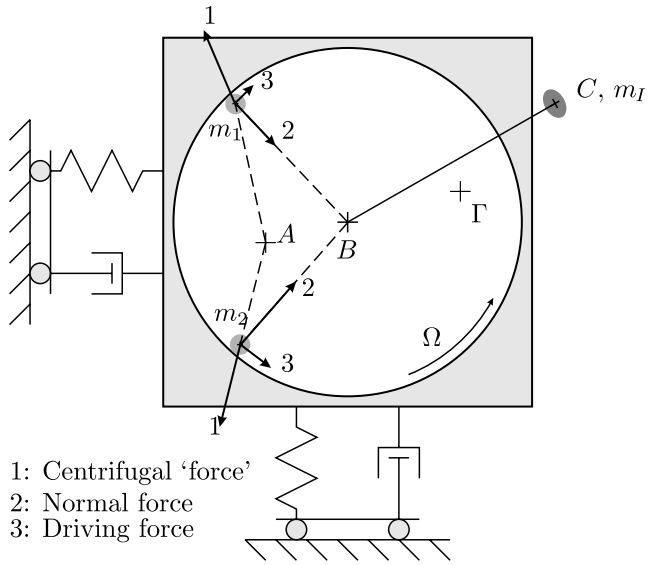

Fig. 6. Interplay of forces; below critical speed.

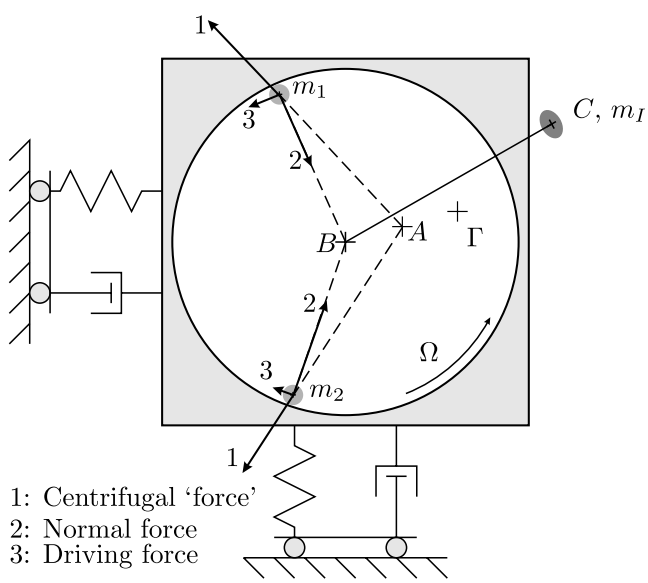

Fig. 7. Interplay of forces; above critical speed.

speed $\mathbf{r}_{B/A} \cdot \mathbf{r}_{\Gamma/B} > 0$, indicating that the angle between both vectors is smaller than $\pi/2$, whereas above the critical speed $\mathbf{r}_{B/A} \cdot \mathbf{r}_{\Gamma/B} < 0$, indicating that the angle between these vectors is larger than $\pi/2$. It should be noted that, when the ABB is isotropically suspended by linear springs and dampers, the critical speed equals the value of both (equal) damped eigenfrequencies $\omega_d = \omega_n\sqrt{1-\zeta^2}$ with $\omega_n = \sqrt{k/M}$ and $\zeta = b/2\sqrt{kM}$; given the parameters in Table 1, $\omega_d = 181.5$ rad/s.

The investigation of the interplay of forces acting on the balls, both below and above the critical speed reveals a remarkable effect. Namely, Fig. 6 shows that the driving force is directed *towards* the imbalance in Γ, thus pushing the balls towards the imbalance and thus enlarging the imbalance. In Fig. 7, however, the driving force points *away* from the imbalance Γ, which results in the balls rolling in such a direction that the resulting imbalance decreases. When the system is completely balanced, points A, B and Γ coincide, the centrifugal and normal forces point in exact opposite direction, cancelling each other. Consequently, the driving force is zero in the balanced situation. This reflects the steady-state solution (equilibrium), for which the system is balanced.

For reasons of simplicity, dissipative effects in the ABB were omitted in the previous analysis of the working principle of the ABB. Nevertheless, these dissipative effects are crucial for the functionality of the ABB, as it is needed that the kinetic energy of the balls is absorbed. This energy dissipation is necessary to obtain asymptotic stability of the ball positions that balance the system [Lee, 1995; Lee & Moorhem, 1996]. In the ABBs discussed in [Lee, 1995] and [Lee & Moorhem, 1996], viscous damping is responsible for the energy dissipation. Such damping can be introduced by filling the ABB with oil or some other viscous fluid. These viscous damping forces are zero in the equilibrium positions and thus the system has (multiple) isolated equilibria, corresponding to a balancing configuration and configurations where the imbalance is not balanced or even increased. Below the critical speed, the balancing equilibrium point is unstable, whereas a nonbalancing equilibrium point is locally asymptotically stable; above the critical speed, the balancing equilibrium point is locally asymptotically stable, whereas the nonbalancing equilibria are unstable. Due to the continuous and differentiable nature of the vectorfield around these equilibria, linearization can provide such (local) stability results.

In the case of the ABB studied in this paper, the dry friction forces between the rim and the balls represent the necessary dissipative forces. However, the essential property of dry friction, which distinguishes it from viscous friction (due to oil), is that it can produce nonzero forces at zero relative velocity between the balls and the ABB. Consequently, the dry friction force can counteract and (exactly) cancel a nonzero driving force, at zero relative velocity. This situation is schematically depicted in Fig. 8, where the shaded areas express possible equilibrium positions of the two balls, which now constitute

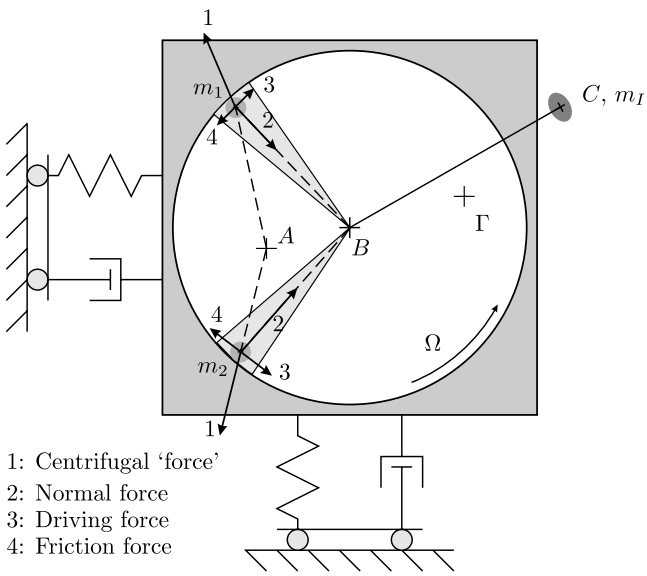

Fig. 8. Interplay of forces with dry friction.

equilibrium sets. In these sets, the friction force exactly cancels the driving force thus ensuring equilibrium. This adaptation of the friction force to the external forces (driving force) is allowed by the set-valued friction law (4); however, the friction force can only cancel forces with an absolute value smaller than $|\mu_i F_{N_i}|$, $i = 1, 2$. This fact defines the boundary of the equilibrium set. It should be noted that F_{N_i}, $i = 1, 2$, depends on the generalized displacements and the generalized velocities. In the next section, the equilibrium sets are studied in more detail.

5. Equilibrium Sets

In this section, the equilibrium sets of the model (2), (3) will be computed and the dependency of these equilibrium sets on the friction parameter μ and the rotational speed Ω will be investigated. More information on the (isolated) equilibria for the system with viscous friction instead of dry friction and the related (local) stability properties can be found in [Van den Heuvel, 2002].

The equilibrium set $\mathcal{E}$ can be found by setting $\ddot{\underline{q}} = \underline{0}$ and $\dot{\underline{q}} = \underline{0}$ in (2), (3). This yields

$$\mathcal{E} = \left\{ (\underline{q}, \dot{\underline{q}}) \in \mathbb{R}^{12} \mid \dot{\underline{q}} = \underline{0} \wedge \underline{q} \in \mathcal{S} \right\}, \tag{6}$$

where

$$\begin{aligned}
\mathcal{S} = \Bigg\{ & \underline{q} \in \mathbb{R}^6 \mid l_1 = L \wedge l_2 = L \wedge \\
& x = \frac{\dfrac{b\Omega}{M\omega_n^2}\left(m_1 \sin(\beta_1) + m_2 \sin(\beta_2)\right) - \left(\left(\dfrac{\Omega}{\omega_n}\right)^2 - 1\right)\left(\dfrac{m_I e}{L} + m_1 \cos(\beta_1) + m_2 \cos(\beta_2)\right)}{\dfrac{M}{L}\left(\left(\dfrac{\Omega}{\omega_n} - \dfrac{\omega_n}{\Omega}\right)^2 + \left(\dfrac{b}{M\omega_n}\right)^2\right)} \wedge \\
& y = \frac{-\dfrac{b\Omega}{M\omega_n^2}\left(\dfrac{m_I e}{L} + m_1 \cos(\beta_1) + m_2 \cos(\beta_2)\right) - \left(\left(\dfrac{\Omega}{\omega_n}\right)^2 - 1\right)\left(m_1 \sin(\beta_1) + m_2 \sin(\beta_2)\right)}{\dfrac{M}{L}\left(\left(\dfrac{\Omega}{\omega_n} - \dfrac{\omega_n}{\Omega}\right)^2 + \left(\dfrac{b}{M\omega_n}\right)^2\right)} \wedge \\
& \left| x \sin(\beta_i) - y \cos(\beta_i) \right| \leq \mu_i \left(x \cos(\beta_i) + y \sin(\beta_i) + L \right), \; i = 1, 2 \Bigg\}.
\end{aligned} \tag{7}$$

In the sequel, the dependency of the equilibrium set, and the consequences in terms of the balancing performance, on two system parameters will be investigated: namely, the friction parameter μ and the rotational speed Ω of the ABB. The friction coefficient is varied to investigate the influence of friction on the magnitude of the equilibrium set. It should be noted that, on the experimental setup, different types of material for both the rim of the ABB and the balls are available: polycarbonate or steel rims and steel, tungsten or brass balls. Each combination of materials will give rise to a different contact situation and thus to different frictional behavior. Previous experiments, see [Van den Heuvel, 2002], showed that the dynamic friction coefficient (quotient between friction force and normal force for nonzero relative velocities) lies in the range $[0.001, 0.01]$ for these different material types. Obviously, the dynamic friction may differ

from the static friction level, but here we merely aim to indicate that the use of different materials gives rise to different friction situations, which justifies the study of the dependency of the behavior of the ABB on the friction coefficient. The rotational velocity is varied to study the effect of this parameter on the equilibrium set and thus on the balancing performance. The resulting knowledge may prove useful when designing startup-profiles for the optical disc drive incorporating the ABB.

Before we discuss these dependencies, let us first show, in Fig. 9, the equilibrium set for a specific parameter setting: $\mu_1 = \mu_2 = 2.75 \times 10^{-3}$ and $\Omega = 216.4$ rad/s; this angular velocity is higher than the damped eigenfrequency $\omega_d = 181.8\,\text{rad/s}$, which ensures that the balancing equilibrium is locally asymptotically stable for a system with viscous friction instead of dry friction. The results in this figure are obtained numerically by defining a grid on the (β_1, β_2)-space, computing on this grid the corresponding equilibrium values for x and y using (7) and finally checking whether the inequalities in (7) are satisfied. This figure illustrates what the effect of dry friction (as opposed to viscous friction) is on the possible equilibrium positions of the balls. Herein, the colored area represents the equilibrium set, which is clearly a large portion of the (β_1, β_2)-space despite the fact that the friction coefficient is very small. The white region corresponds to positions of the balls which are not equilibria. Moreover, the (isolated) equilibrium *points* of the system without dry friction (but with viscous friction) are depicted, where the circles ($\circ$) represent unstable equilibria and the stars ($*$) represent locally asymptotically stable equilibria, which correspond to the balancing equilibrium since $\Omega > \omega_d$. As was expected, these isolated equilibria are contained in the equilibrium set for the system with dry friction (see also schematic Fig. 8). It should be noted that the figure has a symmetry axis at $\beta_1 = \beta_2$ since balls 1 and 2 are identical. The figure is a contour-plot where the colors indicate the magnitude of $a = \sqrt{x^2 + y^2}$, which is the amplitude of the whirling motion which the ABB will perform when the balls are in a specific equilibrium position. The yellow contour line in the figure is a contour line for $a = 2.15 \times 10^{-5}\,\text{m}$ which is the amplitude of the whirling motion when no balls would be present in the ABB; in other words without ABB. Clearly, in the balancing equilibrium points of the system without dry friction (the white stars) $a = 0\,\text{m}$.

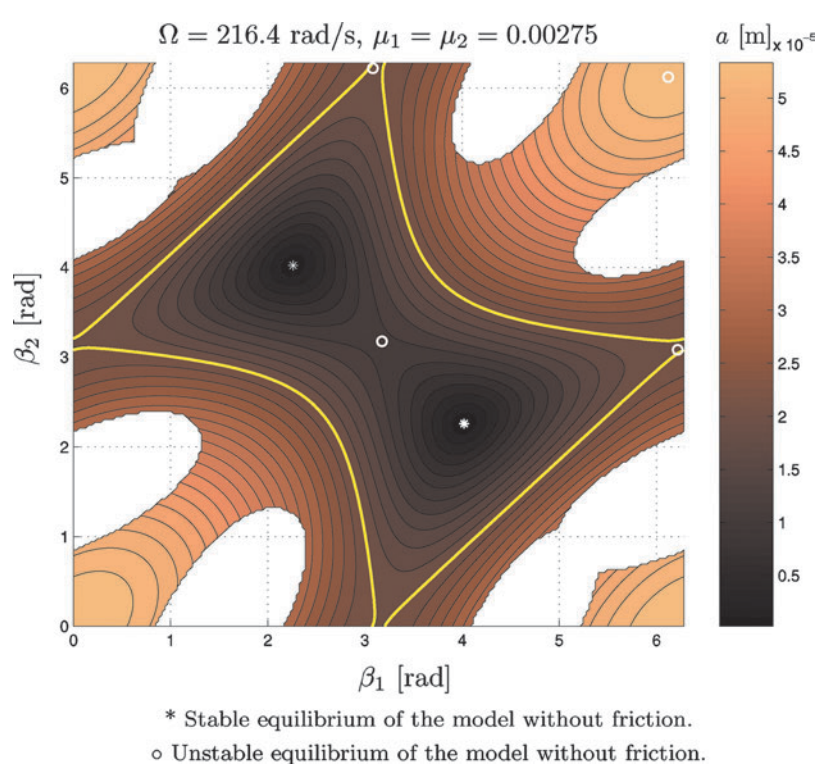

Fig. 9. Equilibrium set for $\Omega = 216.4$ rad/s, $\mu_1 = \mu_2 = 0.00275$.

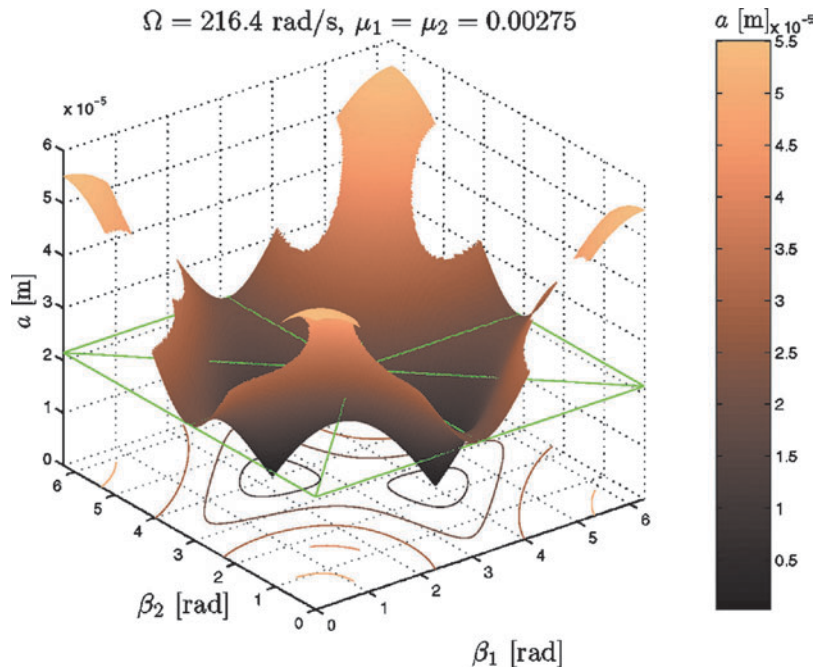

Fig. 10. Vibration amplitudes on the equilibrium set for $\Omega = 216.4$ rad/s, $\mu_1 = \mu_2 = 0.00275$.

In Fig. 10, the relation between the equilibrium position and the resulting amplitude a of the vibration is depicted in a three-dimensional picture for the same parameter values. Herein, the green lines span the plane $a = 2.15 \times 10^{-5}$ m, which again indicates the resulting vibration level without the ABB. The two minima of this plot exactly coincide with the balancing equilibria of the system without dry friction ($a = 0$ m). Figures 9 and 10 clearly show that there exists a large part of the equilibrium set where the application of the ABB leads to a deterioration of the balancing performance when compared to a situation without ABB ($a = 2.15 \times 10^{-5}$ m).

Figure 11 shows the dependency of the equilibrium set with respect to the friction coefficient μ. All equilibrium sets are determined for an angular velocity of $\Omega = 216.4$ rad/s. For a small friction coefficient, the equilibrium set consists of small sets around the equilibrium points of the system without dry friction, see also Fig. 8. As the friction coefficient is increased the equilibrium set grows until it covers the entire (β_1, β_2)-space for still a small value for the friction coefficient: $\mu = 3.5 \times 10^{-3}$. Clearly, only for very small friction coefficients ($\mu = \mathcal{O}(10^{-4})$) the equilibrium set shrinks towards the isolated equilibria of the system without friction. So, even for reasonable small friction coefficients the equilibrium set will be so large that a deterioration of the balancing behavior when compared to the system without ABB can occur ($a > 2.15 \times 10^{-5}$ m). However, it still remains an open question which parts of the equilibrium set are (asymptotically) stable or unstable or which parts are attractive or not. In other words, at this point we do not know *a priori* to which parts (of the equilibrium set) the balls are likely to converge. The answer to that question is ultimately needed to draw final conclusions on the effect of dry friction on the balancing performance of the ABB. In Sec. 6, the static friction coefficient for an ABB with a polycarbonate rim and brass balls is determined experimentally, the corresponding equilibrium set is computed and the implications for the balancing performance are discussed.

Yet another interesting perspective is obtained by varying the angular velocity Ω of the ABB for fixed friction coefficient $\mu = 2.75 \times 10^{-3}$, see Fig. 12. This figure shows that the equilibrium set strongly depends on the angular velocity.[1] More specifically, for low Ω the equilibrium set is large and the stable equilibrium point for the system without dry friction is an equilibrium in which both balls lie close to the imbalance thus enhancing it

[1]It should be noted that the scales of the colorbars in the pictures in Fig. 12 differ from each other.

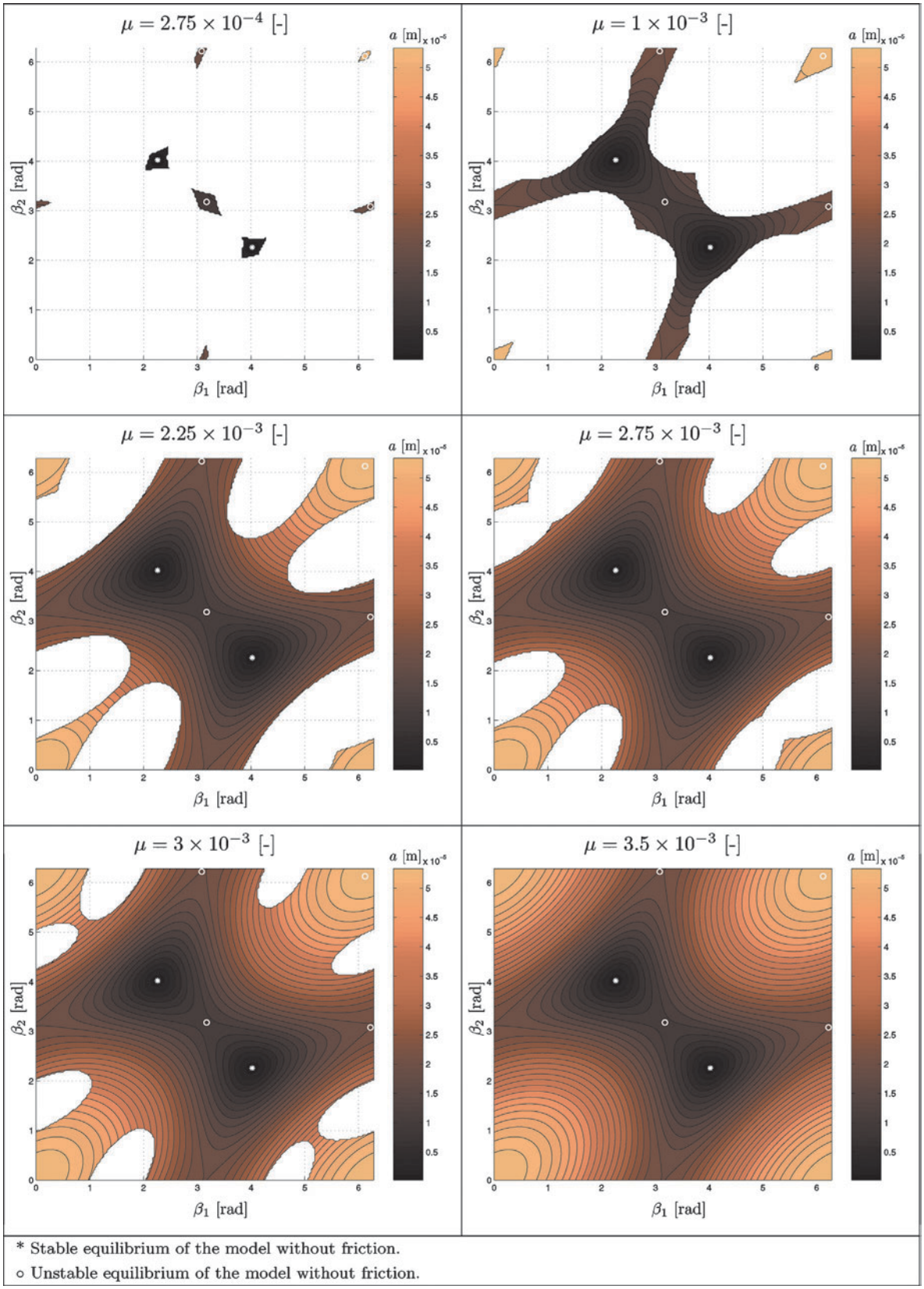

Fig. 11. Equilibrium set for different values of the friction coefficient μ ($\Omega = 216.4$ rad/s).

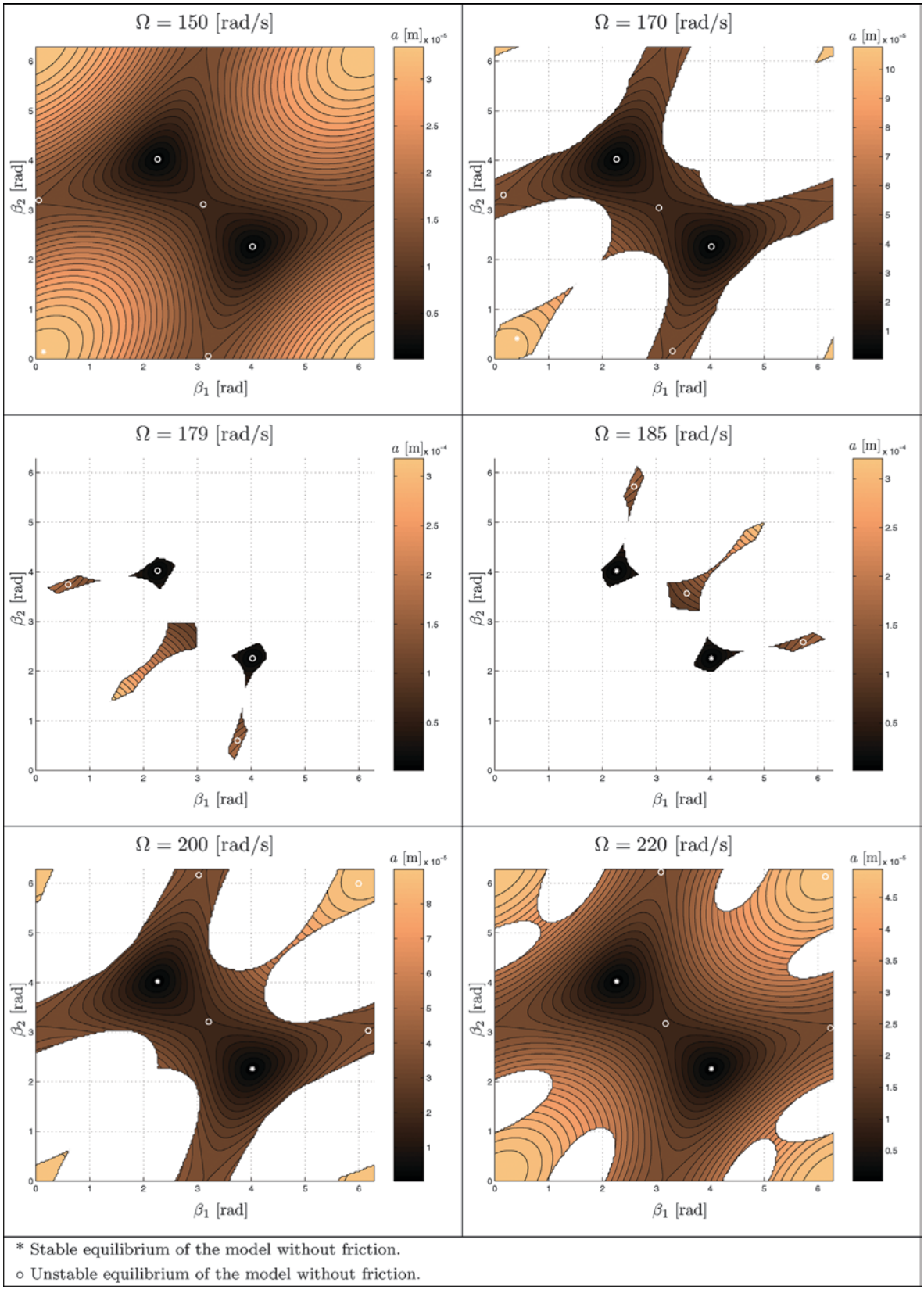

Fig. 12. Equilibrium set for different angular velocities Ω ($\mu = 2.75 \times 10^{-3}$ and $\omega_d = 181.8$ rad/s).

(the latter holds for both $\Omega = 150$ rad/s and $\Omega = 170$ rad/s). When Ω is near the damped eigenfrequency ω_d the equilibrium set shrinks because near resonance relatively high vibrations are caused by the remaining imbalance. Consequently, in Fig. 8, the distance between the points A and B will become large. As a consequence, the angle between a line connecting point A and m_i and a line connecting point B and m_i, $i = 1, 2$, will become larger. This results in a larger tangential component of the centrifugal force (and thus in a larger driving force). The normal force (equal to radial component of centrifugal force) will decrease, resulting in a smaller friction force. As a result of this fact, at more positions of the balls the driving force will exceed the static friction level, thus decreasing the equilibrium set, see Fig. 12 for $\Omega = 179$ rad/s and $\Omega = 185$ rad/s. It should be noted that, for the system without dry friction, for $\Omega = 179$ rad/s no stable equilibrium point exists and that for $\Omega > \omega_d$ the balancing equilibria are stable. As Ω increases above ω_d the equilibrium set grows again since we are moving away from resonance. This can be understood by the following reasoning. For angular velocities higher than the resonance frequency, vibration amplitudes will quickly drop and the driving force will diminish due to the fact that the distance between the points A and B will become smaller (see explanation above). Furthermore, for higher angular velocities the normal force will increase. Consequently, the maximum friction force at zero relative velocity increases, which enables equilibrium at higher driving forces, see friction model (4). Therefore, for such angular velocities the equilibrium set becomes large (see Fig. 12 for $\Omega = 200$ rad/s and $\Omega = 220$ rad/s) and the system is likely to attain an equilibrium.

It should be noted that the operating speed of the CDROM players in which the ABB is used can be as high as $750 - 1100$ rad/s. At such angular velocities the entire (β_1, β_2)-space is an equilibrium set. So, once more we are forced to conclude that an improvement of the balancing performance cannot be guaranteed even for low friction levels. However, in practice (more than two balls are generally involved) the balancing, i.e. the balls finding their balancing equilibrium, occurs during startup relatively close to (and just above) the resonance frequency; thus at much lower angular velocities than the operating speed. Therefore, the angular velocity range studied here is of special interest.

To conclude this section, we will investigate through numerical simulation whether the system is more likely to settle in certain parts of the equilibrium set than in other parts. The purpose of this analysis is to assess the extent to which the balancing performance will indeed improve or deteriorate. Moreover, we will assess the predictive quality of the model by comparison of these numerical results to experimental results. Furthermore, this comparison will support the conclusions on the balancing performance based on the model.

In Fig. 13 the equilibrium set, for $\Omega = 216.4$ rad/s and $\mu = 2.75 \times 10^{-4}$, is compared to numerical simulation results. In order to obtain these results, initial conditions in the set defined by

$$
\begin{aligned}
x(0) &\in [-5.75 \cdot 10^{-4}, 5.75 \cdot 10^{-4}] \quad [\mathrm{m}], & y(0) &\in [-5.75 \cdot 10^{-4}, 5.75 \cdot 10^{-4}] \quad [\mathrm{m}] \\
\beta_1(0) &\in [0, 2\pi] \quad [\mathrm{rad}], & \beta_2(0) &\in [0, 2\pi] \quad [\mathrm{rad}] \\
\frac{dx}{dt}(0) &\in [-0.0209, 0.0209] \quad [\mathrm{m/s}], & \frac{dy}{dt}(0) &\in [-0.0209, 0.0209] \quad [\mathrm{m/s}] \\
\frac{d\beta_1}{dt}(0) &\in [-182, 182] \quad [\mathrm{rad/s}], & \frac{d\beta_2}{dt}(0) &\in [-182, 182] \quad [\mathrm{rad/s}]
\end{aligned}
$$

are used. These initial conditions are taken from a uniform random distribution from this set in order to ensure an even representation of all parts of this set. Subsequently, the differential inclusion (2) was solved numerically for every initial condition. The resulting equilibrium points are depicted in Fig. 13. The numerical procedure is based on an event-driven integration method. The event-driven integration method uses a standard ODE solver for the integration of smooth phases of the system dynamics (neither of the ball's relative velocities $\dot{\beta}_1$ or $\dot{\beta}_2$ are zero). Moreover, once $\dot{\beta}_1$ or $\dot{\beta}_2$ equals zero, the next hybrid mode of the system (stick or slip for each of the balls) is determined. In this case, there are only two discontinuities which allows for

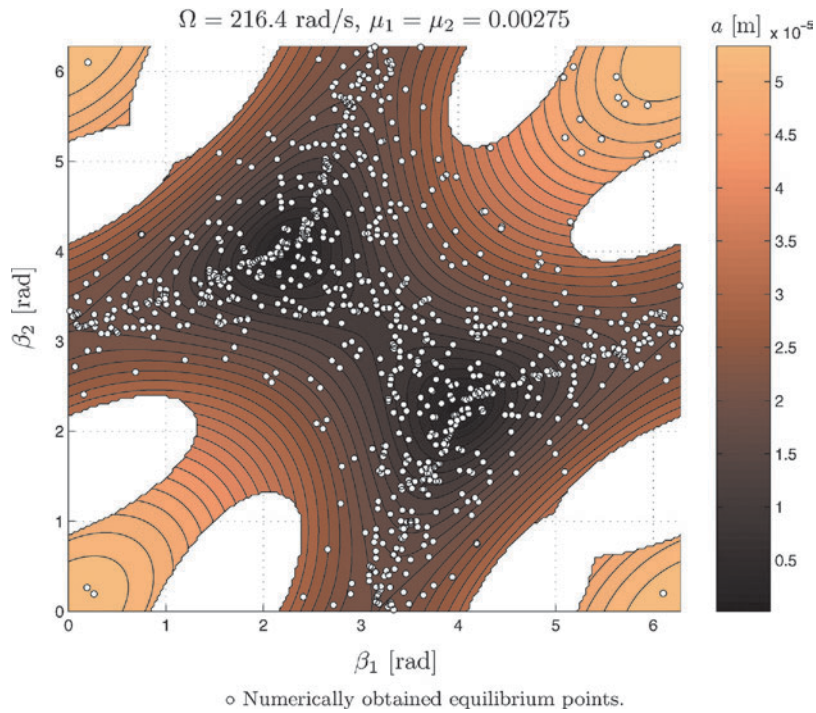

Fig. 13. Numerically obtained equilibrium positions (circles) compared to the modeled equilibrium set ($\Omega = 216.4$ rad/s, $\mu = 2.75 \times 10^{-4}$).

an explicit solution of the combinatorial problem on the discontinuities. However, in general such problems can be formulated as a LCP (Linear Complementarity Problem) and solved numerically in that framework, see [Glocker, 2001]. Figure 13 shows that the numerically obtained equilibria almost completely cover the equilibrium set, which indicates that at least part of the equilibrium set is (locally) attractive. Moreover, it is important to observe that indeed equilibrium points occur in which the balancing is worse than without ABB, which confirms that balancing performance deterioration is not only a possibility but is also likely to occur. Conclusive statements on the attractivity or (Lyapunov) stability of the equilibrium set cannot be made based on these numerical results. In this respect, it should be noted that the stability of equilibrium sets of discontinuous nonlinear systems is a relatively open field of research. In [Van de Wouw & Leine, 2004], sufficient conditions for the attractivity of equilibrium sets for linear mechanical systems with Coulomb friction are presented. However, the extension towards nonlinear systems such as the automatic ball balancer is not trivial.

In Fig. 14, comparable experimental results are shown. Experiments were performed, at $\Omega = 216.4$, for many different initial conditions. The resulting equilibrium positions at which the balls came to rest are depicted in this figure; again with the modeled equilibrium set as a backdrop. This figure shows that also in the experiments equilibrium positions of the balls occur at which the balancing performance is deteriorated compared to a situation without balancing. The resemblance of these experimental and numerical results of Fig. 13 and the fact that the experimental result seems to match well with the equilibrium set of the model may tempt one to conclude that the value of the friction coefficient used in the model matches the real friction coefficient very well. However, careful inspection of these results can only lead to the conclusion that the real friction coefficient is probably larger than 2.75×10^{-4}. Namely, if the real friction coefficient would be smaller, some of the experimentally obtained equilibria would lie outside the (modeled) equilibrium set for this lower μ-value. This would induce a mismatch between model and experiment.

In the next section, an experimental identification of the (static) friction coefficient is discussed and the corresponding modeled equilibrium set is presented. Moreover, a comparison with the experimental results is made and consequences with respect to the balancing performance are discussed.

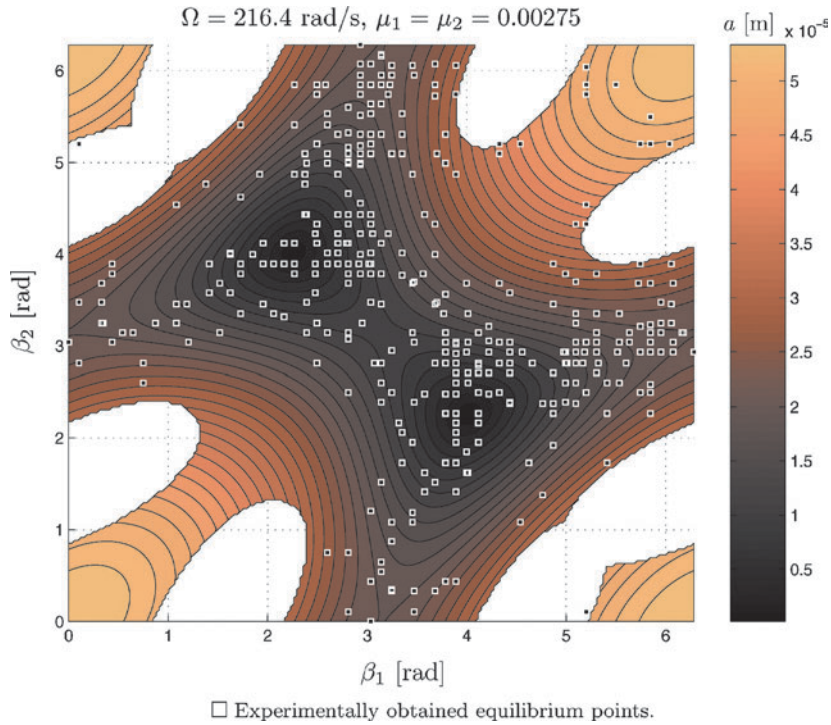

Fig. 14. Experimentally obtained equilibrium positions (squares) compared to the modeled equilibrium set ($\Omega = 216.4$ rad/s).

6. Friction Identification and Resulting Equilibrium Sets

In Sec. 6.1, we will identify the static friction level by means of experiments for a specific combination of material types of the ABB rim and the balls; namely, a polycarbonate rim and brass balls. Subsequently, the equilibrium set of the model with the identified static friction level will be assessed in Sec. 6.2. Moreover, the modeled equilibrium set will be compared to experimentally obtained equilibria and consequences for the balancing performance of the system will be discussed in this section.

6.1. *Friction identification experiments*

In the experiments, in which the static friction level is identified, the table of the ABB is attached rigidly to inertial space and only one ball is used. Consequently, the only degree of freedom of the system is represented by the rotation of the ball with respect to the rim. The experiment follows the following protocol:

- first, the ABB is speeded up to a certain angular velocity. The angular velocity is kept constant until the ball attains a fixed angular position relative to the ABB (the balls are sticking to the rim);
- secondly, an acceleration (or deceleration) profile is prescribed to the ABB, such that after some time the ball starts slipping (attains a nonzero relative velocity with respect to the rim);
- the moment that the ball starts slipping is detected and the angular acceleration ($\dot{\Omega}_{\text{slip}}$) and the angular velocity (Ω_{slip}) are measured.

The moment that the ball starts slipping is detected by measuring both the angular displacement of the ABB and the ball using a high-speed camera, see Fig. 15. Using these measurements, and a dynamic model of the ABB with one ball, the friction force F_T and the normal force F_N at the moment that ball starts slipping can be computed by:

$$F_T = -\left(mL - \frac{2J}{d}\right)\dot{\Omega}_{\text{slip}}, \quad F_N = mL\Omega_{\text{slip}}^2, \quad (8)$$

where m is the mass of the ball, d the diameter of the ball, J the moment of inertia of the ball about its center of mass. Using (8), the friction coefficient μ can be estimated by $\mu = |F_T|/F_N$, since at the moment the ball starts slipping (stick-slip

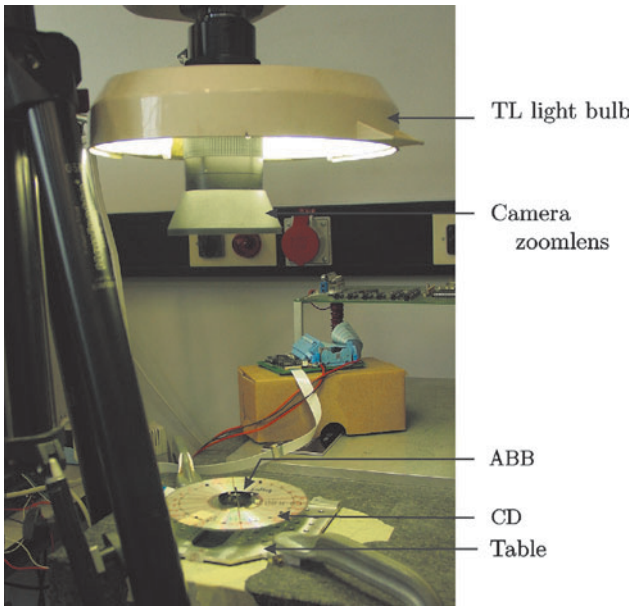

Fig. 15. Picture of the experimental setup with high-speed camera.

transition) the friction force attains its maximum value (for zero velocity). This experiment was performed twelve times and a 95% confidence interval for the friction coefficient was obtained: $0.024 < \mu < 0.035$ with a mean value of 0.03. Clearly, this value for the friction is much higher than the value used in the previous section based on measurements of the dynamic friction level (for nonzero relative velocities). This will result, as will be shown, in an even larger equilibrium set.

6.2. *Resulting equilibrium set*

In Fig. 16, the equilibrium set for the estimated friction coefficient $\mu = 0.03$ and $\Omega = 216.4\,\text{rad/s}$ is shown. The equilibrium set now covers the entire (β_1, β_2)-space; in other words the balls can come to rest at any combination of angular positions in the ABB. It should be noted that this holds for any value of the friction coefficient taken from the 95% confidence interval for the friction coefficient. Clearly, in a large part of the equilibrium set this balancing performance is worse than in the case without ABB. Moreover, in this figure the experimentally obtained equilibrium positions at $\Omega = 216.4$ rad/s are depicted. The comparison of these experimental results with the modeled equilibrium set (see also Fig. 14) leads to the conclusion that the equilibria obtained will not

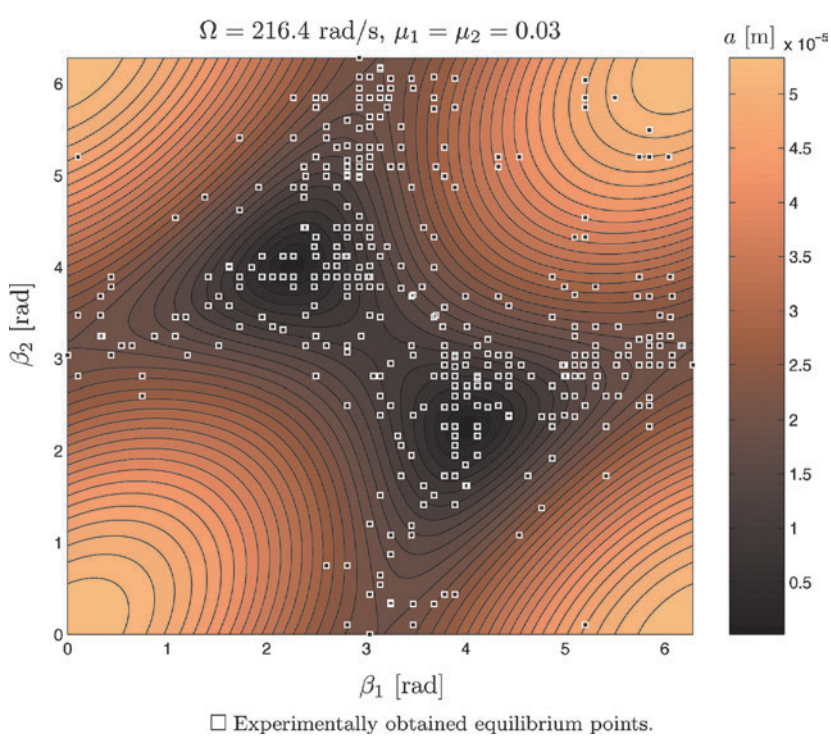

Fig. 16. Equilibrium set for $\Omega = 216.4$ rad/s and $\mu = 0.03$ compared to experimentally obtained equilibrium positions (squares).

necessarily be distributed (evenly) over the equilibrium set. More specifically, there are regions of the equilibrium set in which the system is more likely to settle than in other regions. This raises questions related to the stability and attractivity of equilibrium sets. Firstly, one can doubt whether it is sensible to only argue about the stability/attractivity of the set *as a whole*. Namely, the cause for the fact that the equilibria (experimental) seem to cluster in a specific part of the equilibrium set: can be firstly, the fact that some regions of the equilibrium set are more attractive than others (and the entire set is attractive as a whole) or, secondly, only part of the equilibrium is attractive and another part is not. Consequently, based on these experimental results and the numerical results of the previous section no conclusive statements on the stability/attractivity properties of the equilibrium set of the ABB system can be made. Therefore, further research is needed in this field, because knowledge on these stability/attractivity properties is needed to investigate the exact consequences of the dry friction on the balancing performance in more detail. In this respect, it is important to note that the attractivity and stability properties of the equilibrium set will be influenced by the friction behavior for nonzero velocities, which may very well differ from the Coulomb friction model.

7. Conclusions

The balancing performance of an automatic ball balancer (ABB) with dry friction is investigated. Hereto, a dynamic model of the experimental setup is built and a set-valued Coulomb friction model is used to model the rolling friction between the two balls and the rim of the ABB to account for the stiction phenomenon observed in the experimental setup.

The working principle of the ABB, which leads to balancing, is explained and the way in which the balancing performance is compromised by the presence of dry friction is illuminated. The incorporation of the Coulomb friction model results in the existence of an equilibrium set of ball positions in the ABB. Within part of this equilibrium set the balancing of the vibrations of the system deteriorates when compared to the system without ABB. Consequently, due to the presence of dry friction the balancing performance is seriously compromised.

Furthermore, the dependency of the equilibrium set with respect to the friction coefficient and the angular velocity of the ABB is investigated. It can be concluded that even for very low friction coefficients the balancing behavior can deteriorate. Moreover, only for rotational speeds near resonance the equilibrium set is very small (comprising small sets around the equilibrium points of the system without friction). For rotational velocities outside resonance the equilibrium set grows rapidly. The fact that a wide range of ball positions correspond to equilibria, including combinations of ball positions which induce performance decrease, is confirmed by experimental results.

Dedicated experiments were performed to identify the static friction coefficient for a specific combination of the materials of the balls and the rim of the ABB. The resulting equilibrium set is such that all possible combinations of ball positions are possible equilibria. Consequently, for the experimental setup an improvement of the balancing performance compared to a situation without ABB cannot be guaranteed.

In the simulations (and experiments), the initial conditions were chosen uniformly distributed over a portion of state-space (of which the equilibrium set is a subset), which leads to equilibria which are spread out over the equilibrium set. However, in practice an optical drive is speeded up to its operating speed in a prescribed way. This so-called startup-profile can certainly affect the ultimately obtained equilibria (and thus the balancing performance). A hint towards the design of such a startup-profile can be recognized in Fig. 12. Since the equilibrium set is small for rotational velocities close to resonance, it may very well be desirable to speed up to a rotational velocity just above the resonance frequency (note that the balancing equilibrium point of the system without dry friction is stable for such a rotational velocity). Next, the system can be allowed to settle close to the optimal balancing equilibrium configuration and, finally, it can be speeded up slowly to the operating speed, ensuring that the balls remain (due to dry friction) at the positions attained before.

Finally, the experimental results indicate that some equilibrium points within the equilibrium set seem to be "preferred" over other equilibrium points. This fact raises questions regarding the attractivity/stability properties of (parts of) the equilibrium set. In [Van de Wouw & Leine, 2004], this question is addressed for linear mechanical

systems with Coulomb friction. The extension towards nonlinear systems such as the ABB is an important subject for further research, since knowledge on these attractivity/stability properties will allow us to judge the impact of dry friction on the balancing performance in more detail.

References

Bövik, P. & Högfors, C. [1986] "Autobalancing of rotors," *J. Sound Vibr.* **111**, 429–440.

Childs, D. [1993] *Turbomachinery Rotordynamics*: *Phenomena*, *Modeling and Analysis* (Wiley-Interscience, Chichester).

Chung, J. & Ro, D. [1999] "Dynamics analysis of an automatic dynamic balancer for rotating mechanisms," *J. Sound Vibr.* **228**, 1035–1056.

Chung, J. & Jang, I. [2003] "Dynamic response and stability analysis of an automatic ball balancer for a felxible rotor," *J. Sound Vibr.* **259**, 31–43.

Glocker, Ch. [2001] *Set-Valued Force Laws*, *Dynamics of Non-Smooth Systems*, Lecture Notes in Applied Mechanics, Vol. 1 (Springer-Verlag, Berlin).

Gorbenko, A. [2003] "On the stability of self-balancing of a rotor with the help of balls," *Strength of Materials* **35**, 305–312.

Huang, W.-Y., Chao, C.-P., Kang, J.-R. & Sung, C.-K. [2002a] "The application of ball-type balancers for radial vibration reduction of high-speed optic drives," *J. Sound Vibr.* **250**, 415–430.

Huang, W.-Y., Chao, C.-P. & Sung, C.-K. [2002b] "An intelligent control scheme for enhancing performance of the automatic ball-type balancer installed on high-speed optical disc drives," in *Proc. IEEE Int. Symp. Intelligent Control*, *Vancouver*, *Canada*, pp. 19–24.

Lee, J. [1995] "An analytical study of self compensating dynamic balancer with damping fluid and ball," *Shock Vibr.* **2**, 59–69.

Lee, J. & Moorhem, W. V. [1996] "Analytical and experimental analysis of a self-compensating dynamic balancer in a rotating mechanism," *ASME J. Dyn. Syst. Measur. Cont.* **118**, 468–475.

Lindell, H. [1996] "Vibration reduction on hand-held grinders by automatic balancing," *Central European J. Public Health* **4**, 43–45.

Rajalingham, C. & Rakheja, S. [1998] "Whirl suppression in hand-held power tool rotors using guided rolling balancers," *J. Sound Vibr.* **217**, 453–466.

Thearle, E. [1950] "Automatic dynamic balancers," *Mach. Des.* **22**, 119–124.

van de Wouw, N. & Leine, R. [2004] "Attractivity of equlibrium sets of systems with dry friction," *Int. J. Nonlin. Dyn. Chaos Engin. Syst.* **35**, 19–39.

van den Heuvel, M. [2002] "Modeling and analysis of an automatic balancing unit with dry friction," Master's thesis, Eindhoven University of Technology, Department of Mechanical Engineering, The Netherlands.

Wettergren, H. [2001] "Auto-balance anisotropic mounted rotors," in *Proc. ASME DETC Pittsburgh*, *PA*, *USA*.